8-2024

SURFACE PATTERNING ON ZIRCONIA DENTAL IMPLANTS VIA LASER-INDUCED SHOCKWAVE IMPRINTING

Inomjon Majidov
Western Kentucky University, inomjonmajidov01@gmail.com

SURFACE PATTERNING ON ZIRCONIA DENTAL IMPLANTS VIA LASER-INDUCED SHOCKWAVE IMPRINTING

A thesis submitted in partial fulfillment of the requirements for the degree
Master of Science

Department of Physics and Astronomy
Western Kentucky University
Bowling Green, Kentucky

By
Inomjon Majidov

August 2024

SURFACE PATTERNING ON ZIRCONIA DENTAL IMPLANTS VIA LASER-INDUCED SHOCKWAVE IMPRINTING & Inomjon Majidov

Date Recommended 7/22/2024

DocuSigned by:
ali oguz er
F0511F8EF47B4C8...
Chair

Signed by:
Ivan Novikov
D1F15C9383BB48E...
Committee Member

Signed by:
Jasminka Tirzic
0EE1B5293BD7483...
Committee Member

Committee Member

DocuSigned by:
Jennifer Hammonds
EBE3858E068F42D...
Interim Director of the Graduate School

ABSTRACT

SURFACE PATTERNING ON ZIRCONIA DENTAL IMPLANTS VIA LASER-INDUCED SHOCKWAVE IMPRINTING

Zirconia is rapidly becoming a preferred alternative to titanium in dental applications, primarily due to its aesthetic resemblance to natural teeth. This material's tooth-like color avoids the aesthetic issues associated with the grey metal tint of titanium implants. Additionally, zirconia is hypoallergenic, making it an ideal choice for patients with metal sensitivities or allergies. Despite these advantages, zirconia generally exhibits lower biocompatibility and osseointegration compared to titanium implants. This study investigates laser-assisted, controlled imprinting technique on zirconia surfaces to enhance these properties. Our research used zirconia pellets, produced from powdered monoclinic zirconia pressed in a pellet press machine. Two methods were employed to achieve suitable pattern depth and fidelity using a 1064 nm Nd-YAG laser operating at a 10 Hz frequency. Patterning methods were applied to monoclinic, pre-sintered, and tetragonal (sintered) zirconia samples. Each experimental parameters were controlled to achieve high precision in the pattern formation. Produced patterns were analyzed using Scanning Electron Microscopy (SEM), Atomic Force Microscopy (AFM), and X-ray Diffraction (XRD). These analyses provided comprehensive insights into the morphology, topography, and structural characteristics of the patterned zirconia surfaces. We were able to produce patterns ranging in size from 7 μm to 50 μm in mesh size and depth of up to 2 μm. XRD analysis shows primarily monoclinic zirconia in powder form, primarily tetragonal at 1450 ºC sintering and 50-50 monoclinic and tetragonal phase for zirconia at 1200 ºC sintering. In addition to morphological analysis, the impact of the patterned surface on protein adsorption was also assessed. Protein adsorption has risen by 1.92, when 27% of the surface was patterned. Adsorption increased by

2.69, with 36% of surface patterned. Direct proportionality of adsorption to surface patterns, suggests enhanced bioactivity. This is particularly relevant for improving osseointegration, as higher protein adsorption can facilitate better cell attachment and growth. This study illustrates the potential for the use of laser technology for enhancing dental material properties, contributing effectively to developing zirconia implants that offer better aesthetic and functional characteristics.

Keywords: Dental implant, Laser-assisted surface patterning, Shockwave propagation, zirconia sintering, 3D shockwave imprinting

I dedicate this thesis to my grandfather.

ACKNOWLEDGMENTS

First and foremost, I extend my deepest gratitude to Dr. Ali Er for his unwavering support, mentorship, and patience throughout my graduate research. His guidance has been invaluable. I am also grateful to Dr. Terzic and Dr. Dinan for granting me access to their lab equipment and generously taking the time to teach me how to use it. A special thanks goes to Dr. John Andersland from the biology department, whose continuous assistance and immense knowledge have been an incredible resource. I thank Dr. Novikov for his openness in sharing insights about the research life, which has been enlightening. I would like to acknowledge my lab mate, Yaran Allamyradov, for his help, reassurance, and punctuality. My gratitude extends to Zikrulloh and Salizhan for their early support in teaching me the ways of science. Additionally, I thank Berdimyrat, Imam, and Sajjad for their friendship and willingness to lend a helping hand whenever needed.

Finally, I am deeply thankful to my family for their endless sacrifices, which have allowed me to pursue my degree. Their unwavering support has been the foundation of my achievements. Above all, I thank God for granting me the ability to learn, comprehend, and achieve my goals.

CONTENTS

LIST OF FIGURES

Chapter 1

INTRODUCTION

1.1 Dental Zirconia Implants

Zirconia has gained significant popularity in the past decade as a material for dental implants, serving as an alternative to traditional titanium implants[1–3]. This trend is driven by zirconia's superior aesthetic qualities and its robust physical properties. Zirconia implants are preferred for their natural tooth-like color, which avoids the aesthetic issues associated with the grey metal tint of titanium implants, particularly in patients with thin or receding gums[4]. Additionally, zirconia is hypoallergenic, making it an ideal choice for patients with metal sensitivities or allergies[5,6] .

A biocompatible implant would not only reduce the risk of an allergic reaction, but it will also enhance osseointegration, the process in which the implant and the bone integrate with each other[7–9]. This integration is crucial for the stability and longevity of an implant. Osseo integrative properties of zirconia implants are inferior compared to titanium ones[10–12]. Though zirconia is resistant to corrosion and plaque formation, which helps oral hygiene and prevents risks of gum disease, it will not offer the same level of longevity and sturdiness as titanium. We are working to produce improvements in this area of dental zirconia implants, through laser-assisted controlled patterning. It has been shown that patterning on the surface of implants increase bone to implant adhesion. By increasing surface area and creating uneven surface texture, the cells have a better grip and more area to adhere[13,14].

Laser-assisted surface micro structuring has been shown to yield positive outcomes, as it demonstrated improvement in osteoblast cell adhesion[15]. Additionally, improvements in implant

adhesion and integration were observed with femtosecond pulsed laser micro structuring of zirconia surface[16]. In a more recent study, the laser-assisted patterning on dental zirconia implants highlighted the enhancements in surface damage resistance and surface hardness[17]. Although all of these studies have shown improvement in key characteristics of dental zirconia implants, scalability is still a challenge. Laser ablation, Laser-Induced Periodic Surface Structures (LIPSS), and Laser Interference Lithography (LIL) are methods commonly employed in these studies. Due to the uncontrolled nature of the micro structuring being conducted, localized properties of the material would vary, as the patterns are never the same. In this study, we aim to utilize laser-assisted imprinting to produce controlled surface patterns and to control the surface characteristics of zirconia implants[18]. In this way, we will be able to control and replicate the properties of zirconia implants on a wider scale. The findings from this research could be used in a plethora of fields in homeland security, ranging from aerospace to microelectronics. Surface modifications of aircraft components, improved aerodynamics, decreased friction, and increased resistance to wear and corrosion. At the same time micropatterning the surface of an aircraft makes it hydrophobic and improves the thermal management of the aircraft[19]. Additionally, laser patterning can be utilized in creating intricate, hard-to-duplicate patterns on currency, passports, ID cards, and other critical documents to enhance their security and reduce counterfeiting risks[20].

1.2 Laser - Material Interactions

Understanding the physical phenomena taking place during laser-material interaction will allow for determining suitable techniques for laser-assisted patterning. Laser-material interaction under different pulse lengths of a given laser and material can lead to different results. Depending on the duration of a laser pulse, the mechanism involved in the interaction of a laser with materials could be photothermal, photochemical, hydrodynamical, or ultrafast laser interaction.

Photothermal laser interaction heats the material, causing melting or vaporization, while photochemical laser interaction causes chemical reactions without significant temperature shift[21–23]. Hydrodynamical laser interaction causes fluid-like behavior in materials due to intense heating, and ultrafast laser interaction uses a femto-picosecond pulsed laser to induce precise modifications without thermal diffusion. The different routes of processing have their advantages and disadvantages, making them suitable for different applications based on the required precision, accuracy, and thermal effects[24].

In nanosecond laser-matter interaction, the ablated material is formed in the plume of a plasma. The visible and near-infrared laser radiation mean free path is only up to hundred nanometers in metals; therefore, it represents a very thin layer of material that absorbs the energy of the laser pulse. The rapid deposition of energy confines thermal diffusion to just a few hundred nanometers in the interaction zone, producing a steep temperature gradient that heats and vaporizes the material. After the ablation event, the material vaporized gets ionized by the following laser pulses, creating a highly dynamic plasma plume[25,26] (Figure 1).

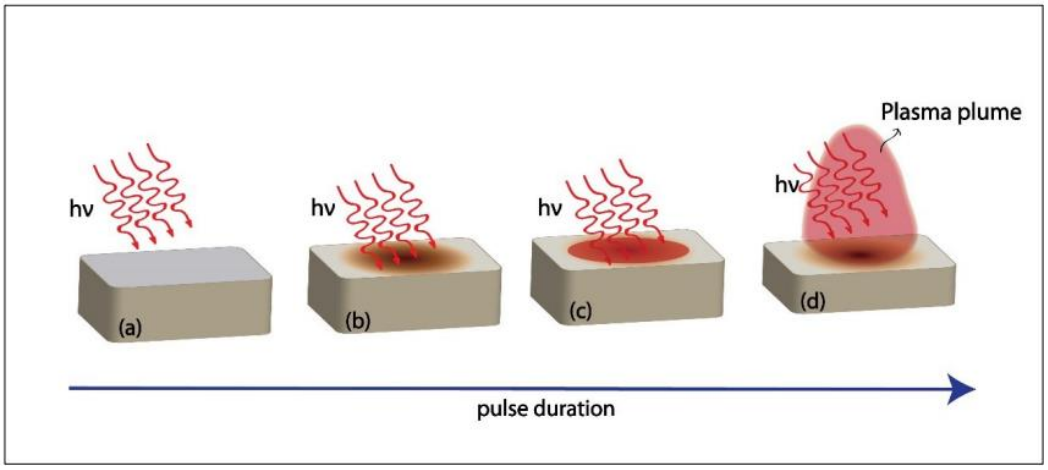

Figure 1. Formation of plasma plume over time via laser-matter interaction

Properties of a laser-produced plasma, such as ionization degree and temperature, change rapidly depending on several aspects: laser wavelength, repetition rate, pulse duration, material

composition, and laser fluence[27]. The plasma continues further to absorb laser energy, raising its temperature to an extremely high value in an extremely short time due to inverse-Bremsstrahlung absorption. As a result of this process atom ionizes and forms the plasma[28].

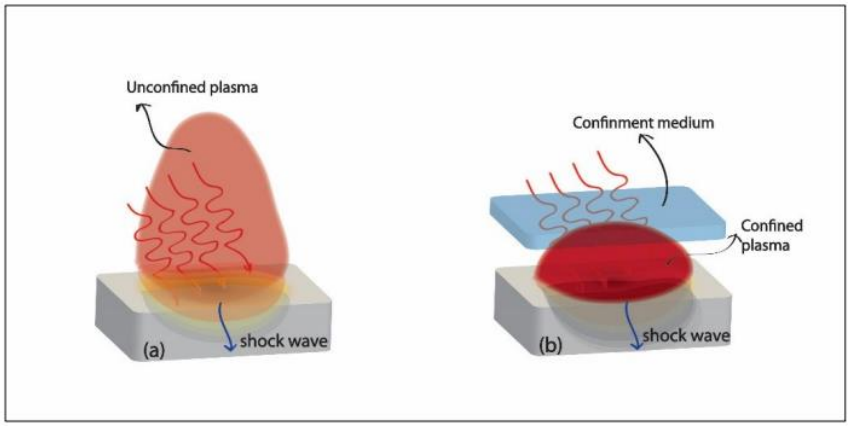

Figure 2 (a) Unconfined and (b) confined shockwave generation.

The solid to vapor transition point in the material generates a shock wave that travels through the sample. A further transparent overlay can increase surface pressure up to 9-fold and help avoid losses from gas breakdown[26], Figure 2. When the shockwave interacts with the surface and is of higher magnitude than the Hugonoit Elastic Limit (HEL) of the material, it plastically deforms it. HEL is a measure of the maximum stress a given material can withstand without any structural modifications[29]. Since zirconia ceramic has a large HEL value compared to metals, it will need a higher-pressure buildup[30]:

$$P = 0.01\left[\frac{Z * I_0 * \delta}{2\delta + 3}\right]^{1/2} \qquad \text{Equation 1}$$

I_o (GW/cm^2) ~ Incident laser power density,

P (GPa) ~ Pressure

Z (g cm^{-2}s^{-1}) ~ Reduced acoustic impedance between a target and medium

δ ~ Efficiency of plasma material interaction.

An increase in I_o, laser intensity, leads to higher pressure buildup. The two other factors namely, δ and Z, are intrinsic properties by themselves. We found that copper has a higher rate of shockwave attenuation, relative to other metals. Z is an acoustic impedance, which depends on the material density and speed of sound in the medium, affecting the shockwave propagation in it. Higher acoustic impedance would suggest more pronounced patterns[31]. Due to this effect, using glass, a higher acoustic impedance material, would be better than water. However, the drawback of using glass is the inability to completely vacuum seal it on the surface. Air has 0.002% acoustic impedance of water, thus it will distort the final pattern if not fully removed[32–34].

1.3 Laser-Assisted Surface Imprinting

Laser-assisted surface imprinting is a transformative technique that utilizes laser technology to create precise and controlled patterns on various materials, including zirconia. This technique involves using a pulsed laser to imprint a template onto the surface of a material, altering its surface properties. In our research, we utilized an Nd-YAG laser operating at a wavelength of 1064 nm, with a frequency of 10 Hz and fluences ranging from 1 J/cm² to 12 J/cm². The pulsed laser interacts with the surface of the material creating an upward-shooting plasma plume[35]. This plasma plume is confined using a glass slide, pressed firmly against the surface. Due to plasma being confined in a tight space, localized high pressure and temperature buildup were observed, with T being upwards of 6500 K and P upwards of 8 GPa at 2J/cm^2. 6500 K temperature buildup is hotter than the surface of the sun, while 8 GPa is equivalent to an elephant on a stiletto heel[36]. These extreme conditions result in plastic deformation of the material and the imprinting of the template, also called laser-induced shockwave imprinting. This method allows for the formation

of patterns with specific dimensions and depths, proportional to the template utilized, critical for applications that require high precision and control. By adjusting parameters such as fluence, exposure time, and beam size, we can achieve patterns with different shapes and sizes, ranging from 7 μm to 40 μm in mesh size and up to 2 μm in depth. These precise patterns are crucial in allowing us to reproducibly alter and enhance the biocompatibility of dental zirconia implants.

By laser micro structuring dental zirconia implant surface using a pre-selected template, we aim to achieve improvements in its dental properties, including osseointegration, biofilm resistance, and longevity. In this study, we explored two methods for laser-assisted surface patterning of monoclinic (non-sintered), pre-sintered, and tetragonal (sintered) zirconia. The first method involves graphite as the sacrificial layer, placed in between the material surface and the ablative layer. The second method uses aluminum as an ablative layer, placing it over the material surface and copper grid.

Post-processing of zirconia involved a two-stage sintering process: pre-sintering at 1200°C followed by a gradual cooling to 300°C, and then final sintering at 1450°C[37]. This controlled approach ensured the patterns remained intact and uniform, avoiding issues such as melting and deformation during the sintering process[38]. The resulting patterns suggest improvements in surface properties of zirconia, which may facilitate better osseointegration. Thus, the integration of laser-assisted surface imprinting with advanced sintering techniques has shown to be a promising approach to enhancing the performance of zirconia dental implants. We aim to provide a comprehensive understanding of the parameters influencing laser patterning, paving the way for innovations in the field of surface micro structuring.

Chapter 2

Materials and Methods

2.1 Zirconium oxide

Monoclinic zirconia pellets were produced from MSE PRO Monoclinic Zirconium Oxide Nanoparticles, 20 nm to 40 nm, >99.9% purity. The powder would be mixed with PVA 5 wt%, acting as a binding agent. A binding agent is a substance that holds or draws other materials together to form a cohesive whole, providing the necessary adhesive properties to ensure that the mixture remains intact. The resulting mixture was put inside a 13 mm diameter hardened steel dry pressing die set for pellet press under max 8 MPa pressure. The produced zirconia pellet weighed 1 g and 13 mm in diameter in monoclinic form. After being patterned the sample was then sintered in the furnace (MTI KSL-1500x) at 1450 ºC. The diameter of the pellet would shrink to 10 mm during the pre-sintered and sintered stages. Before patterning on pre-sintered and tetragonal zirconia samples, the surface roughness was reduced to 0.05 μm using a Buehler EcoMet 250 Grinder-Polisher with an AutoMet 250 Power head[39]. In addition, we have used commercially available aluminum foil (Reynold Wrap) to serve as an ablative layer. While graphite dry lubricant (Blasters) was used as a sacrificial layer for the first method of patterning. We have used 100 to 2000 mesh size TEM grids made of copper as a template for patterning. A clean micro slide (Sargent Welch), with transmittivity of 84% at 1064 nm, was used as a confinement medium[40]. The laser used for the patterning is an Nd-YAG pulsed laser with 1064 nm fundamental wavelength, 10 Hz frequency, pulse width of 5 nanoseconds, and 6 mm diameter unfocused Gaussian-shaped beam (at $1/e^2$).

2.2 Laser-assisted surface imprinting of zirconia.

We have implemented two different pathways to achieve the surface patterning. Firstly, a thin 10 µm layer of graphite was sprayed using graphite dry lubricant, which would act as a protective layer for the sample, preventing melting and ablation. On top of the graphite layer, a 3 mm diameter copper grid was placed as a template and an ablative layer. As shown in Figure 3a, the whole system was sealed using BK7 glass, that confines plasma generated from the laser-ablative layer interaction[12] (details in Appendix A2).

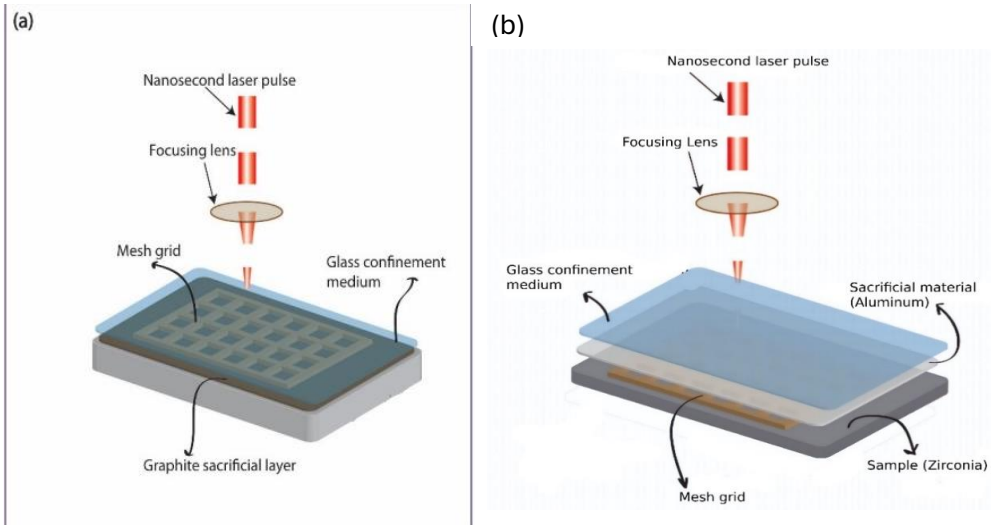

Figure 3. Laser assisted template imprinting experimental setup using (a) "Graphite Method" and (b) "Aluminum Method

The second method uses aluminum foil (Reynold Wrap – Heavy duty) as a sacrificial layer, to protect the material surface from melting and direct laser interaction[41]. A 3 mm diameter copper grid was placed on the surface of zirconia, covered by 16 µm thick aluminum foil (single sheet). As shown in Figure 3b, a BK7 glass was used to seal this system and confine the generated plasma (refer to Appendix A3.).

In the next step, prepared samples were irradiated using selected laser fluences with a focused beam diameter of 3 mm. The expansion of plasma created on the ablative layer was confined using glass slides, which effectively pushed the grid onto the zirconia surface. This

dynamic force induced plastic deformation, resulting in surface patterns that mirrored the holes of the copper grid template[42]. Following irradiation, the copper grid was peeled off, and for samples patterned via the first method, the graphite layer was removed using acetone[43]. Conversely, the second method did not require washing, as the ablation occurred mainly on the aluminum sacrificial layer, leaving the patterned surface clean and undamaged. Additionally, we explored two variations of the original methods for creating patterns. First, using the second method, we placed a copper grid over aluminum foil instead, to serve as an ablative layer. Aluminum foil proved too thick, as copper template was imprinted on it, instead of zirconia. Secondly, using the aluminum method, we applied two layers of aluminum foil as an ablative layer to prevent direct ablation of the material by the laser. The copper template was imprinted on the aluminum foil as it was the softer of the two surfaces and had more to push against.

Morphological properties of the surface were thoroughly investigated using Scanning Electron Microscopy (SEM, Jeol 6510LV) and Atomic Force Microscopy (AFM, Nanosurf Flex AFM). The laser parameters were meticulously adjusted to optimize the protrusion heights, ensuring the patterns achieved the desired depth and uniformity. These analyses provided detailed insights into the pattern fidelity and surface modifications induced by the laser-assisted imprinting process, contributing to a comprehensive understanding of the technique's effectiveness in enhancing the functionality of zirconia implants.

Chapter 3

Results and Discussion

3.1 Patterning on Copper and Nickel plate

As a proof of concept, we applied patterning process on nickel and copper plate. Both the nickel and copper plates used were 1 mm thick. We used the second method with aluminum for patterning, which involves placing a mesh grid between the sacrificial layer and the surface of the sample. The successful imprinting of a hexagonal copper grid on the copper plate was achieved with a single pulse at a fluence of 11.6 J/cm². The resulting pattern exhibited high fidelity and

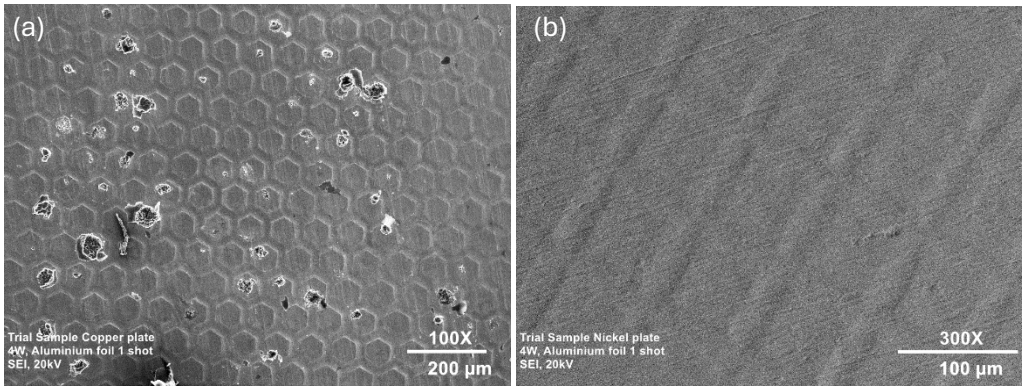

Figure 4 Laser assisted template imprinting with 1 pulse shot at 12 J/cm2 fluence. (a) Nickel plate. (b) Copper plate

uniformity, with a hexagonal grid featuring 698 lines per inch, a hole width of 29 µm, a pitch width of 37 µm, and a bar width of 8 µm, covering a diameter of 3 mm, Figure 4a. Generated patterns were clearly outlined, proportional to the grid dimensions, and visible under both optical microscope and SEM. Although some pieces of the melted copper grid were observed on the surface, they are of no direct importance for this trial.

The images demonstrate that a uniform pattern can be created over a larger area using this method. In the case of the nickel plate, the pattern was also created with a single pulse at 11.6 J/cm² using a square mesh copper grid, Figure 4b. The size, shape, and uniformity of the patterns on both materials using both methods, illustrate the potential for expanding this method to create

patterns over large areas with good reproducibility. By scanning the surface with the laser beam, it would be possible to pattern over a larger area. Additionally, increasing the number of pulses and intensity could produce patterns with greater depth. These trial samples validate the plausibility of producing patterns by imprinting a template and our ability to recreate the given experiment.

3.2 Patterning on Zirconium oxide.

In Figure 5, we can observe three different magnifications of a square grid pattern on the surface of a zirconia pellet. Initially, the zirconia surface was smooth and unblemished. The patterning was attempted using Method 1, which employed a graphite sacrificial layer between a mesh grid and the zirconia surface, Figure 5. After setting up the experimental setup for the first method, we administered 20 laser shots at 1.2 J/cm^2 fluence. The goal is to achieve a uniform, clean, and reproducible surface pattern with high fidelity.

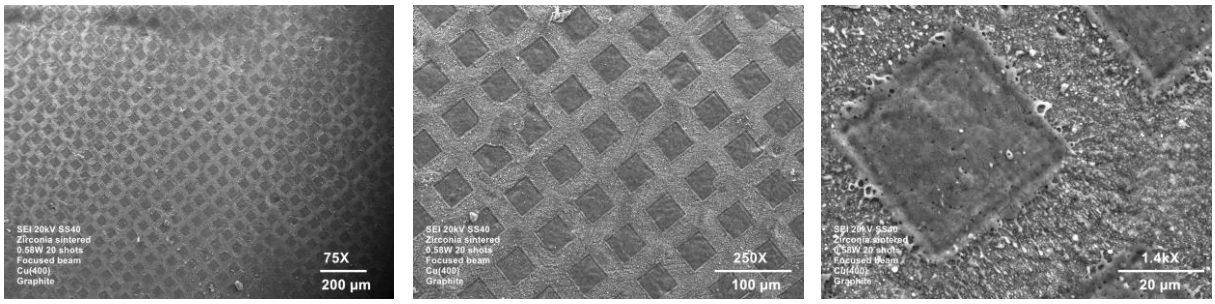

Figure 5 Sintered zirconia surface patterned via "Graphite method."

At a lower magnification of up to 250X, SEM images show a clean imprint of the template grid. Only at a much higher magnification, as can be seen 1.4kX magnification image from Figure 5, small sedimentation on the surface was observed. After elemental analysis of the surface of the square and the pitch, it yielded a similar elemental composition to each other. Zirconia and oxygen content were to be expected, but vast amounts of carbon could only be explained by the presence of graphite. Even though we tried many solvents, including acetone, the graphite was not washed

off completely. At the same time, the AFM image shows some unusual irregularity in the patterned region, Figure 6. Although the data was not conclusive enough, the combination of SEM and AFM images led us to believe that the graphite sacrificial layer was ablated instead of zirconia. The patterns observed using SEM and AFM are the remnants of graphite layer, that was not washed off.

Elt.	Line	Intensity (c/s)	Atomic %	Conc.	Units	Error 2-sig	MDL 3-sig	
C	Ka	1.76	37.72	11.32	wt.%	2.93	2.550	
O	Ka	4.10	27.62	11.04	wt.%	1.66	0.933	
Mg	Ka	0.39	0.17	0.11	wt.%	0.19	0.278	
Si	Ka	1.19	0.35	0.25	wt.%	0.20	0.291	
Ca	Ka	0.06	0.02	0.02	wt.%	0.20	0.303	
Ti	Ka	0.38	0.12	0.15	wt.%	0.24	0.345	
Mn	Ka	0.34	0.13	0.17	wt.%	0.28	0.407	
Fe	Ka	0.58	0.24	0.33	wt.%	0.32	0.451	
Zr	La	114.22	33.63	76.63	wt.%	2.12	0.951	
			100.00	100.00	Wt.%			Total

Table 1.EDS analysis of zirconia surface from Figure 5.

These images collectively demonstrate the shortcomings of the first method, primarily due to the use of a graphite sacrificial layer. The graphite layer, with an average thickness of 15 µm,

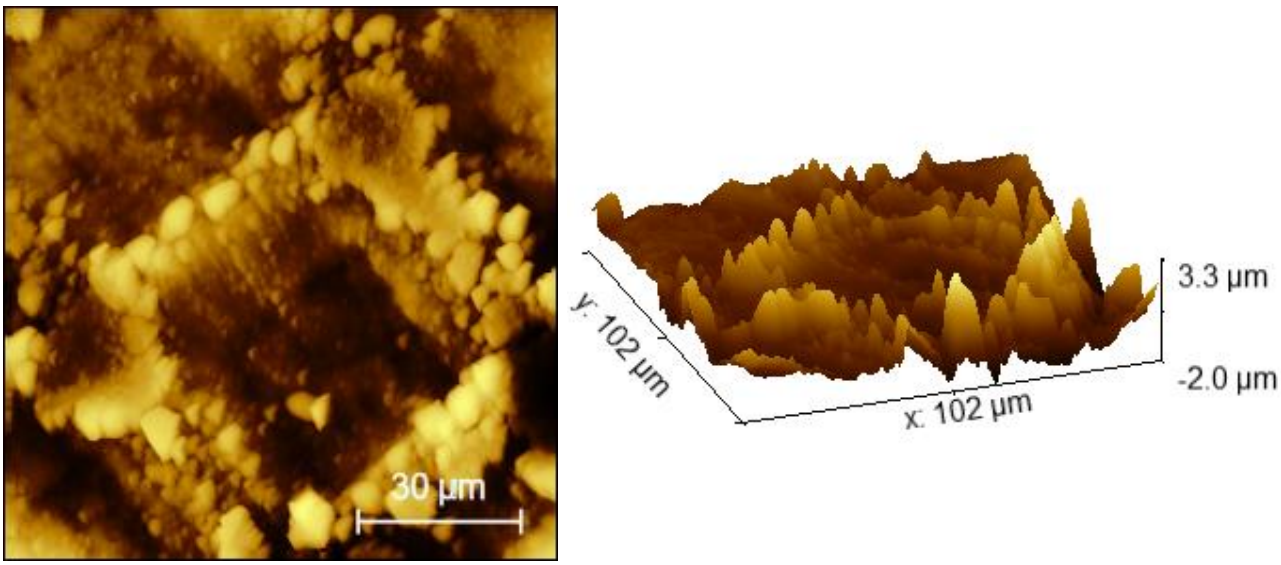

Figure 6 AFM image for patterned zirconia using graphite.

poses significant challenges for the mesh grid to penetrate and accurately transfer the pattern onto the zirconia surface. This limitation results in uneven patterns, as evidenced by the imperfections and irregularities observed in the images.

Given these challenges, we explored an alternative approach to improve the patterning outcomes. Consequently, we propose transitioning to the second method of patterning, which utilizes aluminum as an ablative layer. Aluminum, with its distinct material properties, was anticipated to offer better performance in terms of pattern transfer and resolution. Unlike graphite, aluminum can provide a more effective ablative layer, facilitating a clearer and more precise imprint of the pattern onto the zirconia surface.

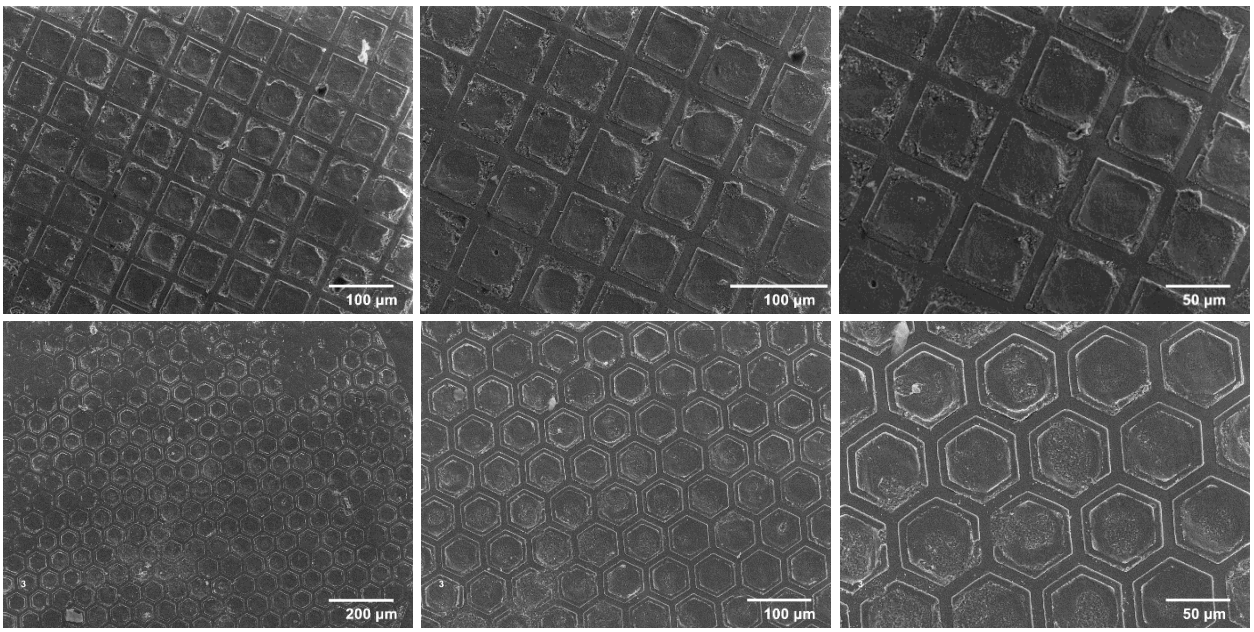

Figure 7 Zirconia surface patterned via "Aluminum method". First row Cu (400) square mesh. Second row Cu (400) hexagonal mesh grid.

Using the second method, we attempted to pattern on tetragonal zirconia, but no discernible pattern emerged. Understanding that zirconia is ceramic and extremely hard, we opted for pre-sintered zirconia, searching for a suitable material that was both soft enough for patterning and sturdy enough to avoid breaking. Unfortunately, the results were underwhelming. We then

experimented with monoclinic zirconia immediately after pressing, before any sintering, which yielded more promising results. The patterns were clear and exhibited a notable degree of uniformity, although some unevenness was present.

The challenge lies in zirconia's inherent hardness and brittleness, making it difficult to deform under pressure. Unlike metals, which can be deformed, zirconia tends to fracture rather than deform. This is highlighted by its Hugonoit Elastic Limit (HEL) of 20-25 GPa, making it nearly as hard as diamond[44]. The HEL measures the maximum stress that a material can withstand under shock-loading conditions before it undergoes plastic deformation. For zirconia, this high HEL indicates significant resistance to deformation, further complicating the patterning process.

For the aluminum method patterning, we conducted experiments that involved creating both square and hexagonal patterns on monoclinic zirconia, which were subsequently subjected to a sintering process. The resulting patterns demonstrated clear delineation and commendable uniformity, which are essential qualities for practical applications, Figure 7.

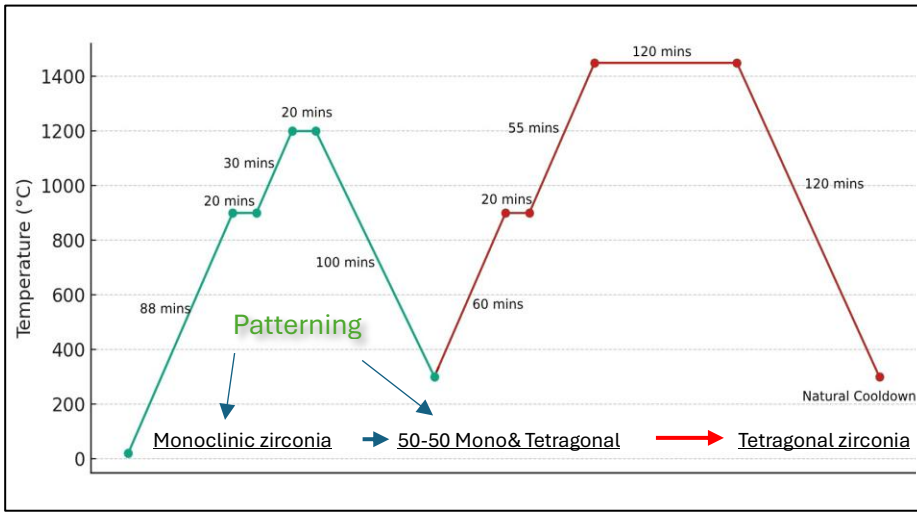

Figure 8. Sintering process for monoclinic zirconia.

The sintering process required careful control to prevent the patterns from degrading or melting. To address this, a two-stage sintering procedure was implemented. Initially, a pre-sintering stage was conducted at 1200°C, followed by a gradual cooling phase to 300°C. This step was crucial as it allowed the patterns to stabilize and adhere more firmly to the zirconia surface. The process for the pre-sintering stage of monoclinic zirconia was developed after numerous trials and errors. Following this, the final sintering was carried out at 1450°C, Figure 8.

This controlled approach ensured that the patterns remained intact and uniform throughout the sintering process. The pre-sintering phase played a vital role in preventing the deformation of patterns, making it possible to achieve the desired quality in the final tetragonal zirconia. Managing the sintering temperatures and cooling phases was critical in maintaining the structural integrity and visual clarity of the patterns. Given these observations, patterning zirconia requires careful consideration of the material's phase and the techniques employed. The success with monoclinic zirconia suggests that patterning at this phase may be the most effective approach, although further optimization is necessary to achieve the desired consistency and precision.

The Atomic Force Microscopy (AFM) images provided offer a detailed examination of the zirconia surface post-patterning. The images include a 2D topographic view, a 3D surface profile, and a depth profile graph, each contributing to a comprehensive analysis of the patterned zirconia, Figure 9.

The 2D topographic image reveals a well-defined hexagonal pattern on the zirconia surface. The hexagons are uniformly distributed, indicating that the imprinting process was executed successfully. Within the hexagonal patterns, the surface roughness appears consistent, which is essential for ensuring the mechanical stability and functional performance of zirconia.

This uniformity is crucial for applications requiring precise surface structuring, such as in the fields of photonics and catalysis.

The 3D surface profile further elucidates the surface topography by providing a perspective on the depth variations within the hexagonal patterns. The color gradient in the 3D image, ranging from dark brown to yellow, indicates depth variations from -1.6 µm to 2.0 µm. The uniformity in depth and shape of the hexagons is particularly notable, as it underscores the efficiency of the method employed. This detailed topography is beneficial for enhancing surface interactions in applications such as surface-enhanced Raman spectroscopy (SERS) or other surface-sensitive techniques.

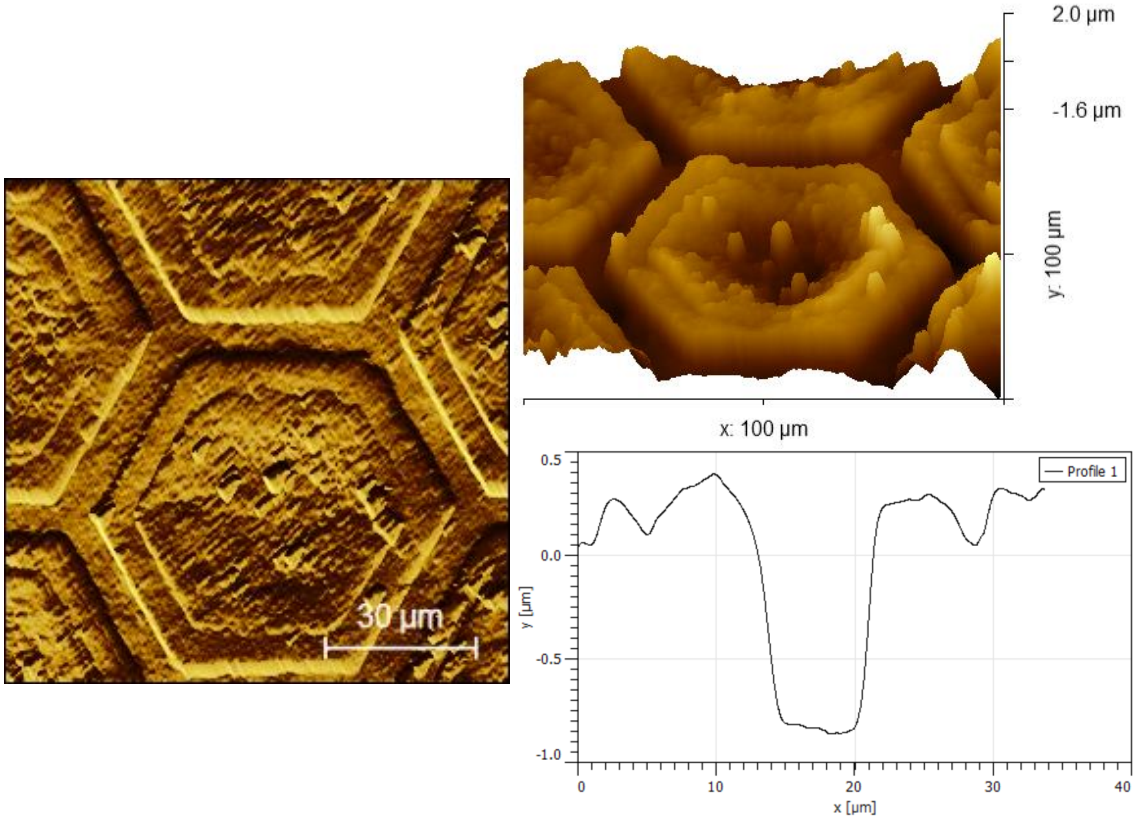

Figure 9. AFM image of a patterned zirconia via aluminum method.

The depth profile graph offers a quantitative analysis of the surface features along a specific line scan. The x-axis represents the lateral distance, while the y-axis indicates the height. The graph

shows distinct peaks and valleys corresponding to the hexagonal pattern, with the deepest points reaching approximately -1.0 μm. This consistency in depth across the pattern suggests a high level of precision. Such uniform depth is vital for reproducibility and reliability in functional applications of the patterned zirconia.

Overall, the images demonstrate that the patterning process on monoclinic zirconia followed by sintering was successful. The patterns are clear, well-defined, and exhibit excellent uniformity. The implementation of a pre-sintering stage at 1200°C, followed by cooling to 300°C before final sintering at 1450°C, appears to have been critical in preventing pattern melting and maintaining the integrity of the imprints. This stepwise sintering process ensures that the patterns remain intact and uniform, crucial for achieving high-quality results.

The success of the patterning, as evidenced by the AFM images, indicates that the process parameters were well-optimized. The hexagonal patterns created using Method 2, involving aluminum, show clear fidelity and structural integrity, making them suitable for various advanced applications. The validation provided by these images supports the hypothesis that pre-sintering stabilizes the patterns, preventing deformation during the final sintering process. This approach has potential implications for the efficient production of patterned ceramic surfaces in both research and industrial settings.

3.3 XRD analysis

The XRD analysis of zirconia at different stages of sintering gives us insight into the nature of phase transition and the structural alteration taking place at different temperatures. This analysis is rooted in the understanding that zirconia exhibits polymorphism, with different phases stable at distinct temperature ranges. Cubic zirconia (c-ZrO2) is stable at temperatures above 2370 °C,

tetragonal zirconia (t-ZrO2) between 1170 °C and 2370 °C, and monoclinic zirconia (m-ZrO2) below 1170 °C[30].

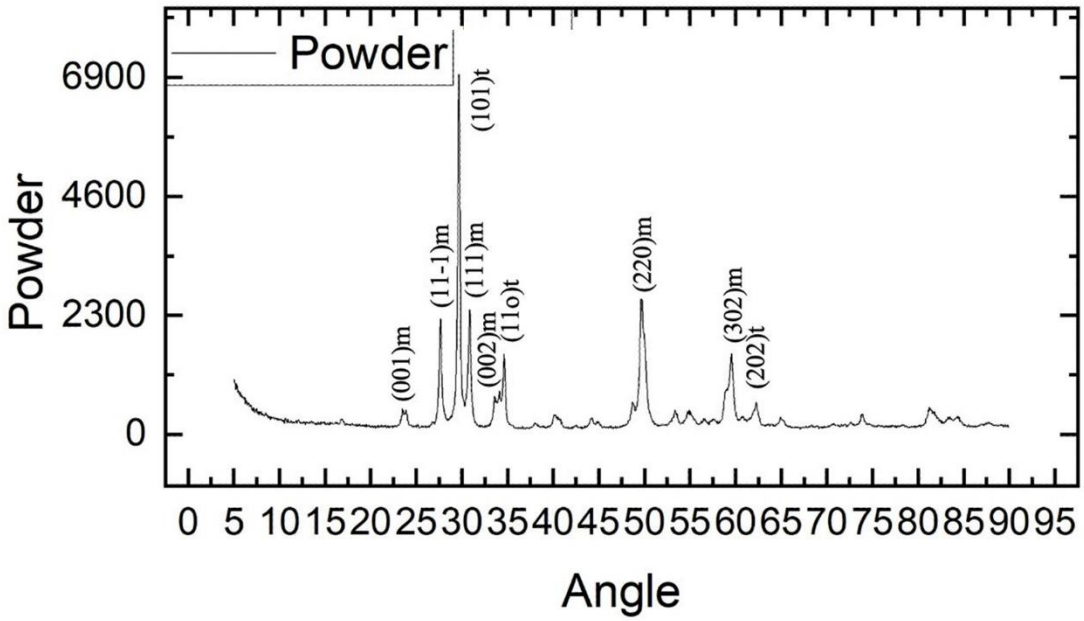

Figure 10. XRD image for Monoclinic zirconia

Figure 10 shows the XRD patterns of zirconia in three forms: monoclinic (powder), monoclinic-tetragonal (pre-sintered), and tetragonal(sintered). The analysis reveals that in its powder form, zirconia predominantly exhibits the monoclinic phase with minor tetragonal phase presence, as indicated by the characteristic peaks in the XRD pattern, Figure 10. This observation is consistent with the fact that the synthesis and storage conditions of the nanopowder did not involve high temperatures that would favor the tetragonal phase.

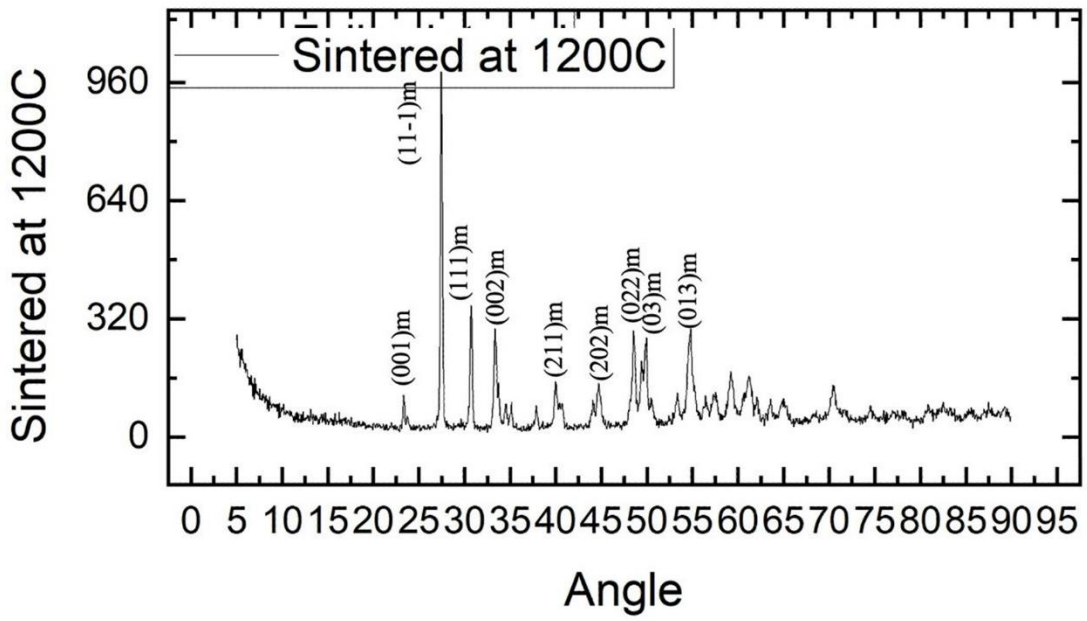

Figure 11. XRD image for pre-sintered zirconia

Upon pre-sintering the zirconia sample, significant changes in the XRD pattern are observed. Some peaks associated with the monoclinic phase decrease in intensity, while others associated with the tetragonal phase become more pronounced, Figure 11. This shift indicates a partial transformation from the monoclinic to the tetragonal phase as the temperature during the sintering process approaches the range where t-ZrO2 is stable. The presence of both phases in the pre-sintered state highlights the incomplete phase transition, which is expected as the thermal treatment has not yet reached the optimal temperature for complete transformation[30].

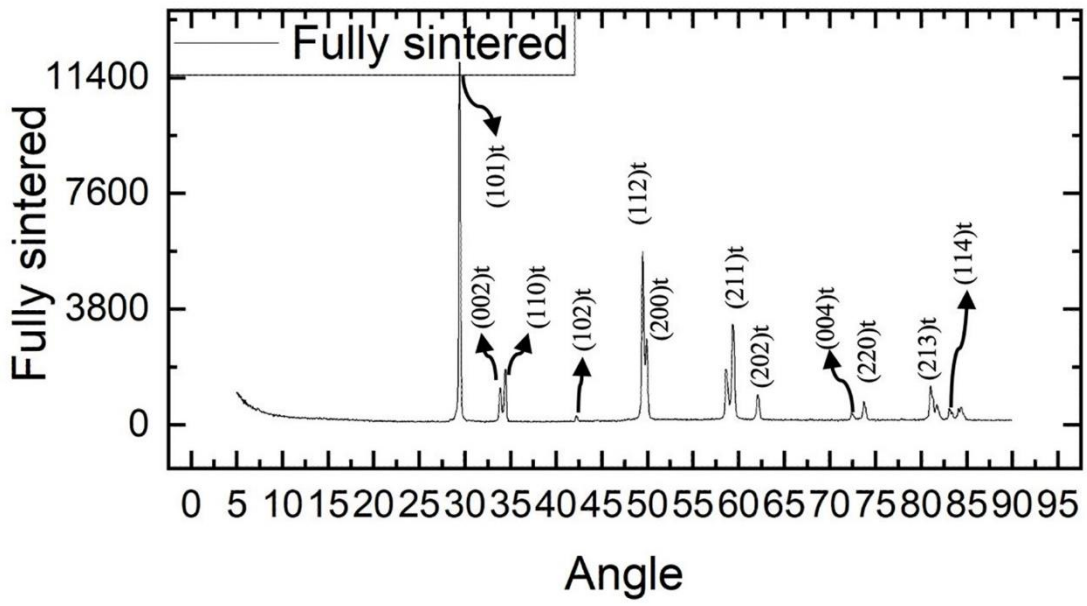

Figure 12. XRD image for Tetragonal zirconia

When zirconia sample is fully sintered at 1450 °C, the XRD pattern reveals the dominance of the tetragonal phase with the disappearance of monoclinic peaks, Figure 12. This transformation aligns with the known phase stability of zirconia, where the tetragonal phase is the most stable form at temperatures between 1170 °C and 2370 °C. The complete phase transition observed in the fully sintered sample demonstrates that the sintering process at 1450 °C provides sufficient thermal energy for the zirconia to transform entirely from the monoclinic to the tetragonal phase. The high intensity and sharpness of the tetragonal peaks in the XRD pattern confirm the crystallinity and phase purity of the tetragonal zirconia[45].

These observations are supported by the theoretical background of zirconia polymorphism. Monoclinic zirconia transforms to the tetragonal phase when heated above 1170 °C, undergoing a martensitic transformation that is associated with significant volume change and shear strain. This

transformation is critical in applications where the mechanical properties of zirconia, are particularly valued, such as in structural ceramics and thermal barrier coatings[45].

The XRD analysis of zirconia in monoclinic, pre-sintered, and tetragonal states elucidates the phase transformations that occur with increasing temperature. The transition from monoclinic to tetragonal zirconia is demonstrated, with the fully sintered sample at 1450 °C exhibiting pure tetragonal zirconia. These findings not only validate the theoretical phase stability of zirconia but also underscore the importance of controlled thermal treatments in achieving the desired phase composition and properties for dental applications.

3.4 Bioanalysis via Protein Adsorption.

In this study, we aim to improve the osseointegration of zirconia implants. Osseointegration is a process by which a bond is formed between living bone tissue and the surface of an implant[7]. To have a better understanding of osseointegration, we have conducted a protein adsorption experiment. We have used Bovine Serum Albumin (BSA) as the adsorbed protein[46]. A 24-well

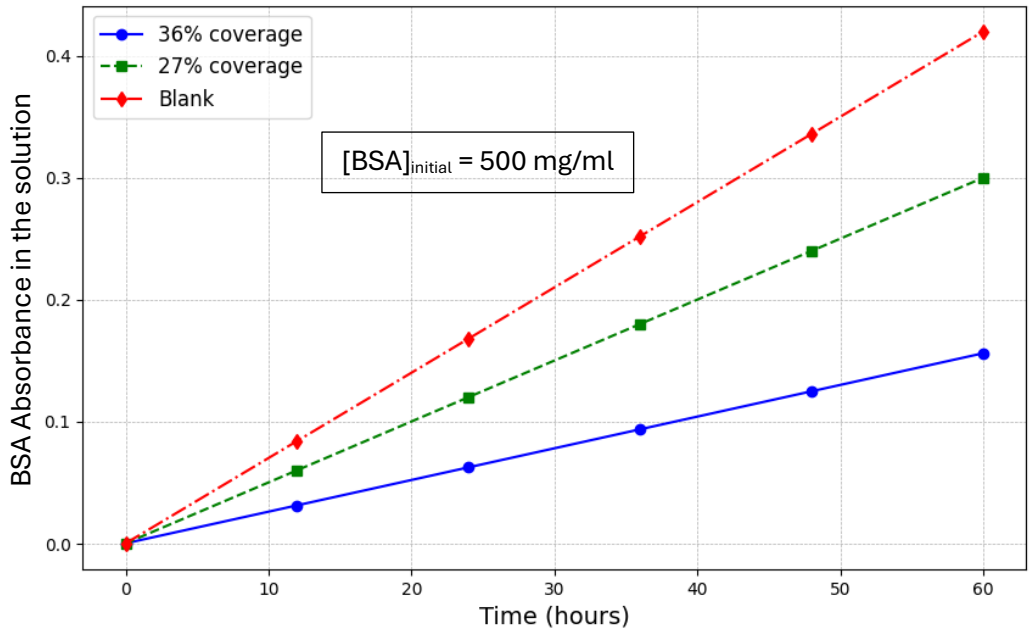

Figure 13. Absorbance vs Time(hours). Zirconia adsorption at different pattern

plate was used to contain all the samples. To prevent BSA adsorption on untreated surfaces, such as the side or the bottom of the pellet, we have used candle wax to cover them. We have done the adsorption at 3 different mediums. 36% pattern coverage, 27% pattern coverage and non-patterned as reference. The concentration of the protein will change over time, due to evaporation and adsorption. To minimize uncertainties, we had 2 identical samples to compare to each other. Every 12 hours, an aliquot of the protein was taken and kept aside. At the end of the experiment, the absorbance spectrum of each aliquot taken was analyzed using a spectrophotometer at 562 nm and the concentration shift was studied against the reference sample. The absorbance slopes for the 36% coverage area of the pattern, 27% coverage area of the pattern, and untreated surface are 0.0026, 0.005, and 0.007, respectively. The 27% surface pattern coverage exhibited a 92% increase in adsorption relative to the reference sample, while the 36% surface pattern coverage exhibited a 169% increase in adsorption. As we can see from the data, the percent surface pattern coverage and adsorption rate are directly proportional. Thus, our results prove the theory that a treated surface would have better protein adsorption. This result is also indicative of a better osseointegration for a patterned surface. Having higher protein adsorption on the surface would lead to an assumption that osseointegration on that surface is more favorable.

CONCLUSION

This study demonstrated the potential and challenges of laser-assisted template imprinting on various materials, including copper, nickel, and zirconia. Using the graphite method, we successfully imprinted hexagonal patterns on copper and nickel plates with a single pulse at a fluence of 11.6 J/cm^2. The resulting patterns, clearly defined and visible under both optical microscopy and SEM, validate the effectiveness of this method in creating precise and uniform patterns over large areas. However, attempts to pattern tetragonal zirconia using the first method,

which involved a graphite sacrificial layer, yielded unsatisfactory results with irregular and poorly defined patterns. Transitioning to the second method, with an aluminum ablative layer showed more promise. Despite zirconia's inherent hardness and brittleness, patterning on monoclinic zirconia before sintering, produced clear and uniform patterns. The implementation of a two-stage sintering process, with pre-sintering at 1200 °C followed by final sintering at 1450 °C, proved critical in maintaining pattern integrity, highlighting the importance of controlled thermal treatment.

XRD analysis provided further insights into the phase transformations of zirconia under different thermal treatments. Powdered zirconia predominantly exhibited the monoclinic phase, with minor tetragonal presence. Upon pre-sintering, a partial transformation to the tetragonal phase was observed. Fully sintered zirconia at 1450°C displayed pure tetragonal zirconia, confirming the theoretical phase stability and underscoring the significance of precise thermal management to achieve the desired phase composition and properties.

In addition to structural analysis, our bioanalysis using protein adsorption experiments with Bovine Serum Albumin (BSA) indicated that patterned zirconia surfaces exhibited higher protein adsorption rates compared to non-patterned surfaces. The absorbance slopes for the 36% surface pattern coverage, 27% surface pattern coverage, and untreated surfaces were 0.0026, 0.005, and 0.007, respectively, suggesting that surface patterning enhances protein adsorption. This finding is indicative of improved osseointegration potential for zirconia implants.

Overall, this research demonstrates the feasibility and effectiveness of laser-assisted template imprinting, particularly the method involving aluminum as an ablative layer, in creating precise and uniform patterns on various substrates. However, further optimization is necessary to refine the patterning process, especially for challenging materials like zirconia. Future work should

focus on fine-tuning the parameters and exploring additional materials to expand the applicability of this technique, ultimately enhancing its potential for advanced technological and biomedical applications.

APPENDIX A: Sample Preparation

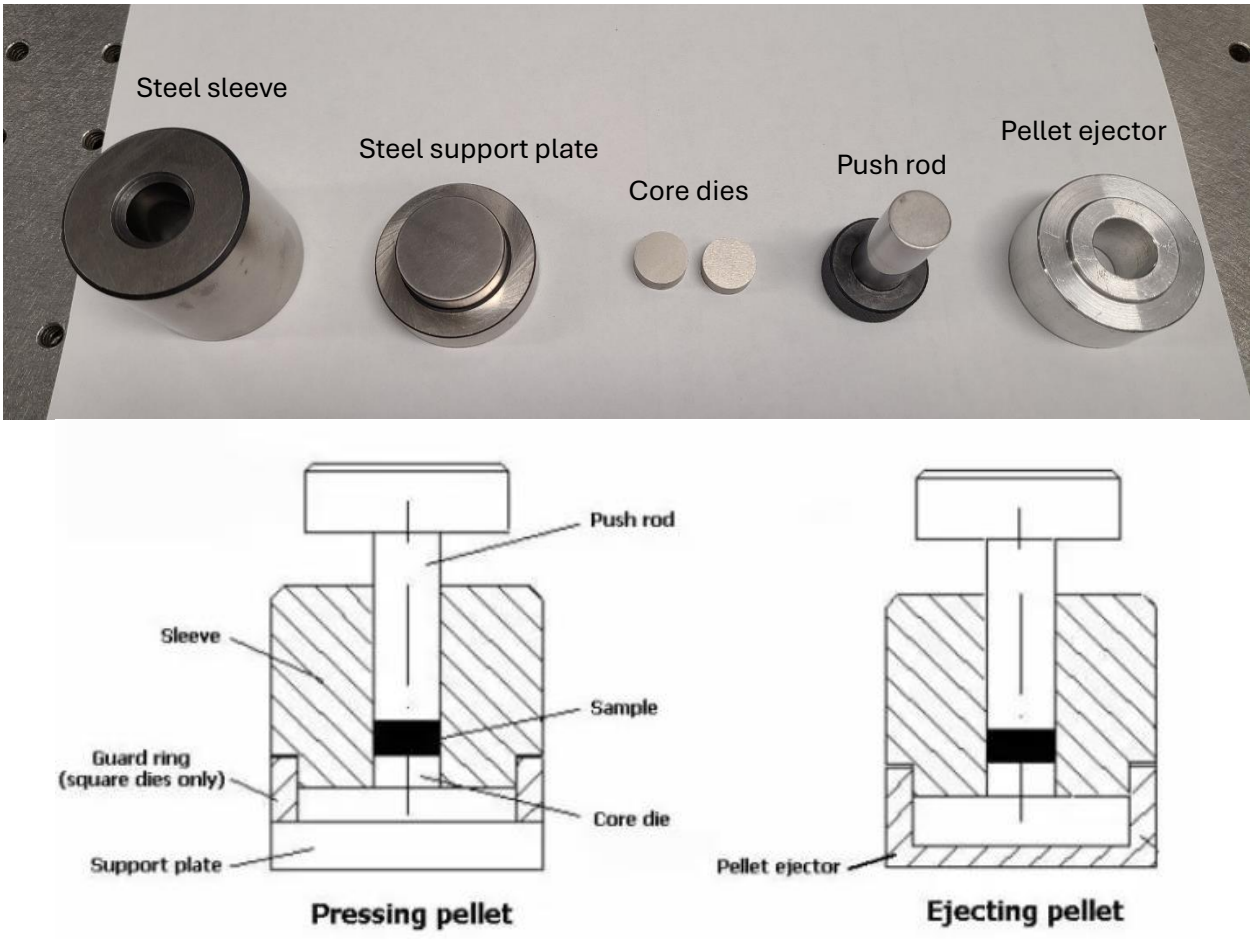

Figure 14. Individual parts of a pellet press and the outline of a setup

A1. Zirconia sample preparation

We have prepared sintered zirconia discs of 1 cm diameter, from powdered monoclinic zirconia.

1. Place MSE PRO Monoclinic Zirconium Oxide Nanoparticles in a beaker.
2. Add 50 µl 5 wt% PVA solution per 5 g of zirconia powder. Mix it well. The time interval between this step and the next, should not be more than an hour.
3. Set up the dry press die set for the pellet press.
4. Place the steel sleeve on the steel support plate.
5. Insert a single die in the hole of a steel sleeve.
6. Weigh 1 g of the mixture and pour it in.

7. Place the second die over it.
8. Insert the push rod and gently press on it.
9. Place this setup inside the hydraulic pressing machine (Carver), Figure 15.

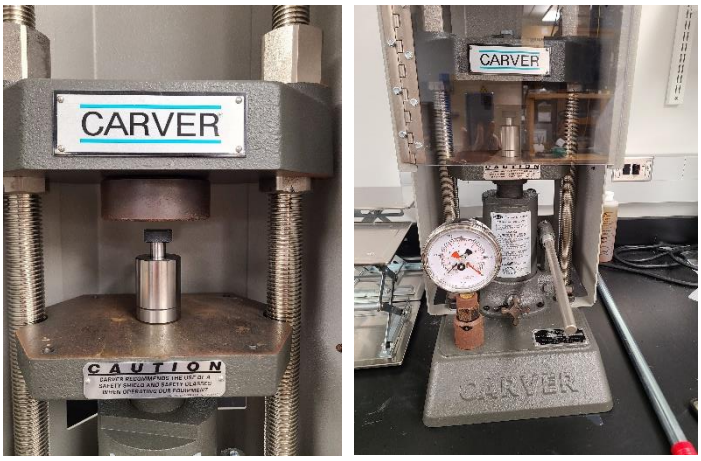

Figure 15. The die set inside the hydraulic pressing machine.

10. Close the hydraulic press valve and start pumping. Make sure the hydraulic press door is closed for safety purposes.
11. Stop after reaching 8 MPa pressure. Wait for 10 mins.
12. Very slowly open the valve to decrease the pressure.
13. Remove the system from the hydraulic press.
14. Replace the support plate with the pellet ejector.
15. Flip the system on its head and put it inside the hydraulic press.
16. Close the valve and start pumping, slowly.
17. This is needed to push the pellet out of the lower half of the system, thus make sure to hold the body. It will drop suddenly, once the samples are out.
18. Remove the sample using tweezers and open the valve.
19. Clean the pellet press die set using ethanol and sanding paper, very thoroughly.
20. If continuing, repeat the process.
21. If finished, clean the die set and let it dry. After it is dry place it back into its case.

22. Sinter the produced pellet at 1450ºC for full sintering.

A2. Sample Preparation using Method 1

1. Place the pellet on a paper towel. Spray the graphite by moving it in a single direction, once. Hold the spray approximately 10 cm away and it will produce a graphite layer of around 10 μm on the sample.
2. Let the graphite dry on the surface and place the mesh grids on top.
3. Place the sample on a piece of transparent heavy-duty tape. Remove the static charge on the tape beforehand.
4. Cut a 2x2 cm square piece of glass from pre-cleaned glass slides from Sargent Welch. Make sure the glass doesn't have any cracks, as it would sabotage the pressure buildup. Clean it with acetone and kimwipes. Place it on a piece of transparent heavy-duty tape.
5. Using a razor blade, cut and remove a piece of tape, that would be covering the surface to be patterned. Laser beams will be interacting at those spots and having a tape, will add unnecessary variables.
6. Take the tape with a glass piece and slowly place it on the tape with the sample. Make sure the sticky sides are facing each other and firmly press them together. The resulting system must be airtight and have minimal separation of the sample surface and glass piece. The sample is ready for patterning under Method 1.

A3: Sample preparation using Method 2

This sample preparation uses aluminum as an ablative surface instead of the mesh grid. In this design, we have used aluminum foil as both the sample and the ablative surface.

1. Cut a suitable-sized glass piece (glass slides from Sargent Welch). This glass will be the confinement medium. Clean the glass piece before use using acetone and kimwipes.
2. Place the mesh grid on the pellet sample. If the sample is thinner than 5 mm, use a second piece of glass as the base.
3. On top of the sample with the mesh grid on it, place the aluminum foil (heavy-duty Reynolds).
4. Put the sample pellet with the mesh grids on transparent tape.
5. Put the glass piece on the piece of transparent tape, as well.
6. Place the glass piece on the sample pellet. Stick it together and make airtight.
7. Cut out the tape piece that covers the area of laser mesh grid interaction. The sample is ready for patterning using the second method.

APPENDIX B: Nd-YAG Laser Operation

Turn ON Procedure:

1. **Laser Safety Protocol**

- Before turning ON the laser, everyone in the lab must wear laser protective goggles and be aware that the laser is being turned on.

2. **Turning On the Laser**

- Rotate the key counterclockwise to turn on the laser, Figure 16. Wait 10 seconds for the water flow to start.

Figure 16. Initial turn on procedure of a laser.

3. **Shutter Safety**

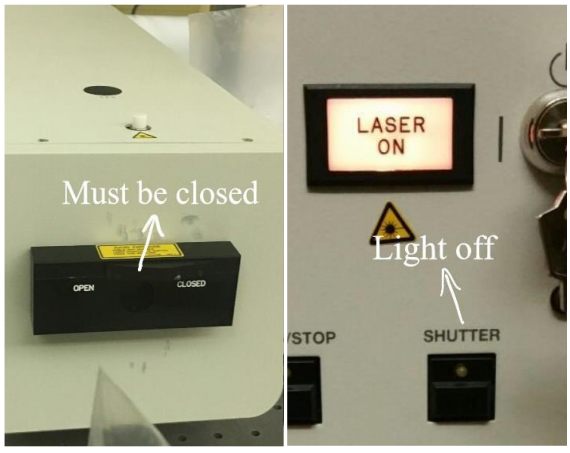

Figure 17. Shutter on the laser head (left) and the shutter button on laser controller (right)

- Ensure all laser shutters are closed before starting. Close the shutter in front of the laser; the laser light should be off, Figure 17.

4. **Laser Settings**

- Use the SELECT button to toggle between laser settings. Adjust the Q-switch value: increasing the Q-switch decreases power and vice versa. The Q-switch must not go lower than 200 to avoid detrimental effects. For most laser patterning experiments, set the Q-switch to 250.

5. **Starting the Laser**

- Press the START button located near the shutter button on the laser controller. The light will turn on and blink, indicating the laser has started, accompanied by a continuous clicking sound.

6. **Operating Modes**

- For continuous pulse (P01) or single shot (P00) mode, press the SELECT button until the P01 reading appears on the laser controller screen, Figure 18, indicating continuous pulse mode.

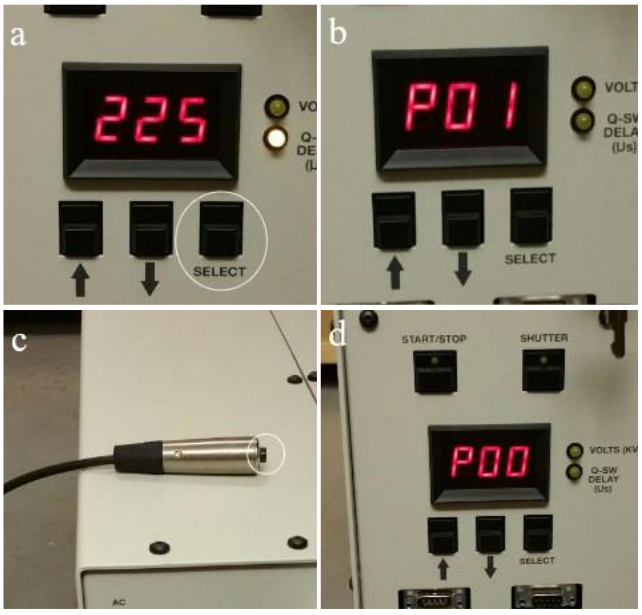

Figure 18. Summary of the procedure for single shot mode, a) press the SELECT button multiple times until b) P01 appears, c) press the single shot button once, d) P01 will change into P00. Single shot cable

7. **Changing Modes**

- To switch from continuous pulse to manual single shot mode, press the button on the single shot cable once, changing the P01 to P00, Figure 18. Starting the laser in P00 mode is always safer.

8. **Warm-Up Period**

- Allow about 15 minutes for the laser to warm up and stabilize.

9. **Safety Check**

- STOP! Ensure everyone is wearing safety goggles.

10. **Opening the Shutter**

- Open the shutter at the front of the laser by sliding it to the left, Figure 19.

Figure 19. Opening the shutter on the front of the laser.

11. **Path Check**

- STOP! Follow the expected path of the laser beams to ensure safety and that the laser does not hit any equipment in the lab.

12. **Adjusting Laser Energy**

- To adjust the laser energy, use the half-wave plate and polarizer, Figure 20. Rotate the half-wave plate to adjust energy levels, decreasing energy for one beam while increasing the other.

13. **Beam Management**

- The beam will split into two components by the polarizer: one in the direction of the initial beam and one perpendicular. Block the unused beam with a beam dump.

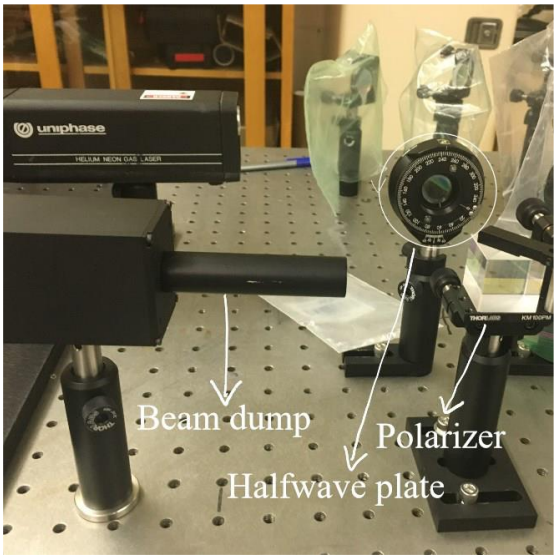

Figure 20. Beam dump, Polarizer and Halfwave plate.

14. **Power Meter Adjustment**

- Position the power meter on the side of the polarizer to be used. Adjust its height so the laser hits the center.

15. **Activating the Laser**

- Ensure safety, then open the shutter by pressing the shutter button on the laser controller, Figure 17. The shutter button light will turn on.

16. **Laser Control**

- The laser is now on and controlled by the single shot button (P00 mode). Press the button once for a single laser beam; press and hold for 5 seconds for continuous beams at the preset frequency (P01 mode).

17. **Energy Adjustment**

- Adjust the laser energy to the desired value by rotating the half-wave plate either counterclockwise or clockwise.

18. **Stopping the Laser**

- After adjusting the energy, press the single shot button to stop the laser (P00 mode). Align the laser to hit the target.

Turn OFF Procedure:

1. Press the single shot button to stop the laser (P00 mode).
2. Press the SHUTTER button to turn off the laser. The laser light should turn off as well.
3. Slide the shutter in the front of the laser to close it.
4. Turn off the laser by pressing the START/STOP button. The clicking should stop afterward.
5. Rotate the key switch clockwise to turn off the laser.
6. Cover the optics with plastic bags to prevent dust formation. Continuously change the plastic bags to prevent any dirt buildup.

REFERENCES

(1) Özkurt, Z.; Kazazoğlu, E. Zirconia Dental Implants: A Literature Review. *J. Oral Implantol.* **2011**, *37* (3), 367–376. https://doi.org/10.1563/AAID-JOI-D-09-00079.

(2) Osman, R.; Swain, M. A Critical Review of Dental Implant Materials with an Emphasis on Titanium versus Zirconia. *Materials* **2015**, *8* (3), 932–958. https://doi.org/10.3390/ma8030932.

(3) Apratim, A.; Eachempati, P.; Krishnappa Salian, K.; Singh, V.; Chhabra, S.; Shah, S. Zirconia in Dental Implantology: A Review. *J. Int. Soc. Prev. Community Dent.* **2015**, *5* (3), 147. https://doi.org/10.4103/2231-0762.158014.

(4) Pirker, W.; Kocher, A. Immediate, Non-Submerged, Root-Analogue Zirconia Implants Placed into Single-Rooted Extraction Sockets: 2-Year Follow-up of a Clinical Study. *Int. J. Oral Maxillofac. Surg.* **2009**, *38* (11), 1127–1132. https://doi.org/10.1016/j.ijom.2009.07.008.

(5) Zarzar, A. A. Immunologically Neutral Dental Implants Ceramic (Zirconia) Implants. *J. Dent. Oral Sci.* **2022**. https://doi.org/10.37191/Mapsci-2582-3736-4(3)-137.

(6) Monti, L.; Franchi, M.; Ursino, N.; Mariani, I.; Corona, K.; Anghilieri, F. M.; D'Ambrosi, R. Hypoallergenic Unicompartmental Knee Arthroplasty and Return to Sport: Comparison between Oxidized Zirconium and Titanium Niobium Nitride. *Acta Biomed. Atenei Parm.* **2022**, *93* (3), e2022160. https://doi.org/10.23750/abm.v93i3.12677.

(7) Elias, C. N.; Meirelles, L. Improving Osseointegration of Dental Implants. *Expert Rev. Med. Devices* **2010**, *7* (2), 241–256. https://doi.org/10.1586/erd.09.74.

(8) T., A.; C., J. Osteoinduction, Osteoconduction and Osseointegration. *Eur. Spine J.* **2001**, *10* (0), S96–S101. https://doi.org/10.1007/s005860100282.

(9) Parithimarkalaignan, S.; Padmanabhan, T. V. Osseointegration: An Update. *J. Indian Prosthodont. Soc.* **2013**, *13* (1), 2–6. https://doi.org/10.1007/s13191-013-0252-z.

(10) Bosshardt, D. D.; Chappuis, V.; Buser, D. Osseointegration of Titanium, Titanium Alloy and Zirconia Dental Implants: Current Knowledge and Open Questions. *Periodontol. 2000* **2017**, *73* (1), 22–40. https://doi.org/10.1111/prd.12179.

(11) Depprich, R.; Zipprich, H.; Ommerborn, M.; Naujoks, C.; Wiesmann, H.-P.; Kiattavorncharoen, S.; Lauer, H.-C.; Meyer, U.; Kübler, N. R.; Handschel, J. Osseointegration of Zirconia Implants Compared with Titanium: An in Vivo Study. *Head Face Med.* **2008**, *4* (1), 30. https://doi.org/10.1186/1746-160X-4-30.

(12) Hanawa, T. Zirconia *versus* Titanium in Dentistry: A Review. *Dent. Mater. J.* **2020**, *39* (1), 24–36. https://doi.org/10.4012/dmj.2019-172.

(13) Chakravorty, N.; Jaiprakash, A.; Ivanovski, S.; Xiao, Y. Implant Surface Modifications and Osseointegration. In *Biomaterials for Implants and Scaffolds*; Li, Q., Mai, Y.-W., Eds.; Springer Series in Biomaterials Science and Engineering; Springer Berlin Heidelberg: Berlin, Heidelberg, 2017; Vol. 8, pp 107–131. https://doi.org/10.1007/978-3-662-53574-5_4.

(14) Pellegrini, G.; Francetti, L.; Barbaro, B.; Del Fabbro, M. Novel Surfaces and Osseointegration in Implant Dentistry. *J. Investig. Clin. Dent.* **2018**, *9* (4), e12349. https://doi.org/10.1111/jicd.12349.

(15) Hao, L.; Lawrence, J.; Chian, K. S. Osteoblast Cell Adhesion on a Laser Modified Zirconia Based Bioceramic. *J. Mater. Sci. Mater. Med.* **2005**, *16* (8), 719–726. https://doi.org/10.1007/s10856-005-2608-3.

(16) Delgado-Ruíz, R. A.; Calvo-Guirado, J. L.; Moreno, P.; Guardia, J.; Gomez-Moreno, G.; Mate-Sánchez, J. E.; Ramirez-Fernández, P.; Chiva, F. Femtosecond Laser Microstructuring of Zirconia Dental Implants. *J. Biomed. Mater. Res. B Appl. Biomater.* **2011**, *96B* (1), 91–100. https://doi.org/10.1002/jbm.b.31743.
(17) Zhang, Y.; Lawn, B. R. Novel Zirconia Materials in Dentistry. *J. Dent. Res.* **2018**, *97* (2), 140–147. https://doi.org/10.1177/0022034517737483.
(18) Majidov, I.; Allamyradov, Y.; Kylychbekov, S.; Khuzhakulov, Z. Surface Patterning on Zirconia Dental Implants by Laser Imprinting. In *Laser-based Micro- and Nanoprocessing XVIII*; Kling, R., Pfleging, W., Sugioka, K., Eds.; SPIE: San Francisco, United States, 2024; p 56. https://doi.org/10.1117/12.3001074.
(19) Barshilia, H. C. Surface Modification Technologies for Aerospace and Engineering Applications: Current Trends, Challenges and Future Prospects. *Trans. Indian Natl. Acad. Eng.* **2021**, *6* (2), 173–188. https://doi.org/10.1007/s41403-021-00208-z.
(20) Liersch, I. ID Cards and Passports. In *Smart Cards, Tokens, Security and Applications*; Mayes, K., Markantonakis, K., Eds.; Springer International Publishing: Cham, 2017; pp 387–412. https://doi.org/10.1007/978-3-319-50500-8_14.
(21) Jacques, S. L. Laser-Tissue Interactions: Photochemical, Photothermal, and Photomechanical. *Surg. Clin. North Am.* **1992**, *72* (3), 531–558. https://doi.org/10.1016/S0039-6109(16)45731-2.
(22) Bäuerle, D. Thermal, Photophysical, and Photochemical Processes. In *Laser Processing and Chemistry*; Springer Berlin Heidelberg: Berlin, Heidelberg, 2011; pp 13–38. https://doi.org/10.1007/978-3-642-17613-5_2.
(23) Kompa, K. L. Laser Photochemistry at Surfaces—Laser-Induced Chemical Vapor Deposition and Related Phenomena. *Angew. Chem. Int. Ed. Engl.* **1988**, *27* (10), 1314–1325. https://doi.org/10.1002/anie.198813141.
(24) Khuzhakulov, Z.; Kylychbekov, S.; Allamyradov, Y.; Majidov, I.; Ben Yosef, J.; Er, A. Y.; Kitchens, C.; Banga, S.; Badarudeen, S.; Er, A. O. Formation of Picosecond Laser-Induced Periodic Surface Structures on Steel for Knee Arthroplasty Prosthetics. *Front. Met. Alloys* **2023**, *1*, 1090104. https://doi.org/10.3389/ftmal.2022.1090104.
(25) Pustovalov, V. K. Heating of Nanoparticles and Their Environment by Laser Radiation and Applications. *Nanotechnol. Precis. Eng.* **2024**, *7* (1), 015001. https://doi.org/10.1063/10.0022560.
(26) Ilhom, S.; Kholikov, K.; Li, P.; Ottman, C.; Sanford, D.; Thomas, Z. Scalable Patterning Using Laser-Induced Shock Waves. *Opt. Eng.* **2018**, *57* (04), 1. https://doi.org/10.1117/1.OE.57.4.041413.
(27) Haider, A. J.; Alawsi, T.; Haider, M. J.; Taha, B. A.; Marhoon, H. A. A Comprehensive Review on Pulsed Laser Deposition Technique to Effective Nanostructure Production: Trends and Challenges. *Opt. Quantum Electron.* **2022**, *54* (8), 488. https://doi.org/10.1007/s11082-022-03786-6.
(28) Zohuri, B. Principles of Plasma Physics. In *Plasma Physics and Controlled Thermonuclear Reactions Driven Fusion Energy*; Springer International Publishing: Cham, 2016; pp 45–98. https://doi.org/10.1007/978-3-319-47310-9_2.
(29) Rosenberg, Z. On the Relation between the Hugoniot Elastic Limit and the Yield Strength of Brittle Materials. *J. Appl. Phys.* **1993**, *74* (1), 752–753. https://doi.org/10.1063/1.355247.

(30) Peyre, P.; Berthe, L.; Scherpereel, X.; Fabbro, R.; Bartnicki, E. Experimental Study of Laser-Driven Shock Waves in Stainless Steels. *J. Appl. Phys.* **1998**, *84* (11), 5985–5992. https://doi.org/10.1063/1.368894.
(31) Hiremath, N.; Kumar, V.; Motahari, N.; Shukla, D. An Overview of Acoustic Impedance Measurement Techniques and Future Prospects. *Metrology* **2021**, *1* (1), 17–38. https://doi.org/10.3390/metrology1010002.
(32) Https://Www4.Uwsp.Edu/Physastr/Kmenning/Phys115/Link5-09_acoustic_impedance.Pdf.
(33) Fahy, F. Impedance. In *Foundations of Engineering Acoustics*; Elsevier, 2001; pp 48–73. https://doi.org/10.1016/B978-012247665-5/50005-9.
(34) Https://Www.Bostonpiezooptics.Com/Ultrasonic-Properties. https://www.bostonpiezooptics.com/ultrasonic-properties.
(35) Https://Www.Colorado.Edu/Lab/Ngpdl/Research/Materials-Processing/Interaction-Expanding-Plasma-Plume-Ambient-Gas-Pulsed-Laser-Deposition.
(36) Https://Science.Nasa.Gov/Sun/.
(37) Https://Www.Beautyzir.Com/Products/Zirconia-Block-98mm-Ht.
(38) Oh, G.-J.; Yun, K.-D.; Lee, K.-M.; Lim, H.-P.; Park, S.-W. Sintering Behavior and Mechanical Properties of Zirconia Compacts Fabricated by Uniaxial Press Forming. *J. Adv. Prosthodont.* **2010**, *2* (3), 81. https://doi.org/10.4047/jap.2010.2.3.81.
(39) Https://Www.Metallographic.Com/Metallographic-Preparation-Procedures/Superalloys-Ceramic-Coating.Htm.
(40) Https://Www.Spectroscopyonline.Com/View/1064-Nm-Raman-Right-Choice-Biological-Samples.
(41) Wang, L.; Su, C.; Jia, X.; Guo, Z.; Zou, Z. Experiment and Simulation Study of the Laser-Induced Cavitation Bubble Technique for Forming a Microgroove in Aluminum Foil. *Micromachines* **2023**, *14* (11), 2106. https://doi.org/10.3390/mi14112106.
(42) Yang, R.; Hu, Y. Plastic Deformation Mechanisms and Their Threshold Pressures of Ti6Al4V Thin-Walled Structures Induced by Laser Peen Forming. *Opt. Laser Technol.* **2023**, *167*, 109722. https://doi.org/10.1016/j.optlastec.2023.109722.
(43) Umek, P.; Vrbanič, D.; Remškar, M.; Mertelj, T.; Venturini, P.; Pejovnik, S.; Mihailović, D. An Effective Surfactant-Free Isolation Procedure for Single-Wall Carbon Nanotubes. *Carbon* **2002**, *40* (14), 2581–2585. https://doi.org/10.1016/S0008-6223(02)00170-7.
(44) Cutler, R. A.; Reynolds, J. R.; Jones, A. Sintering and Characterization of Polycrystalline Monoclinic, Tetragonal, and Cubic Zirconia. *J. Am. Ceram. Soc.* **1992**, *75* (8), 2173–2183. https://doi.org/10.1111/j.1151-2916.1992.tb04480.x.
(45) Https://Ri.Conicet.Gov.Ar/Handle/11336/49093.
(46) Putman, B.; Van Der Meeren, P.; Thierens, D. Reduced Bovine Serum Albumin Adsorption by Prephosphatation of Powdered Zirconium Oxide. *Colloids Surf. Physicochem. Eng. Asp.* **1997**, *121* (1), 81–88. https://doi.org/10.1016/S0927-7757(96)03978-7.

Copyright Permission

Name: Majidov, Inomjon

Email (to receive future readership statistics): inomjonmajidov01@gmail.com

Type of document: ['Thesis']

Title: SURFACE PATTERNING ON ZIRCONIA DENTAL IMPLANTS VIA LASER-INDUCED SHOCKWAVE IMPRINTING

Keywords (3-5 keywords not included in the title that uniquely describe content): Monoclinic zirconia, Dental Zirconia, Zirconia sintering, template imprinting

Committee Chair: Dr. Ali Oguz Er

Additional Committee Members: Dr. Novikov, Ivan Dr. Terzic, Jasminka

Select 3-5 TopSCHOLAR® disciplines for indexing your research topic in TopSCHOLAR®: Plasma and Beam Physics Optics Condensed Matter Physics Structural Materials